Electronic Supplementary Material (ESI) for Sustainable Energy & Fuels.

Supporting Information for

Nitrogen-Doped Porous Carbons Derived from Natural Polysaccharide for Multiple Energy Storage

Yongpeng Cui, Huanlei Wang*, Xiaonan Xu, Yan Lv, Jing Shi, Wei Liu, Shougang Chen and Xin Wang

Institute of Materials Science and Engineering, Ocean University of China, Qingdao 266100, China

***** Email:huanleiwang@gmail.com; huanleiwang@ouc.edu.cn.

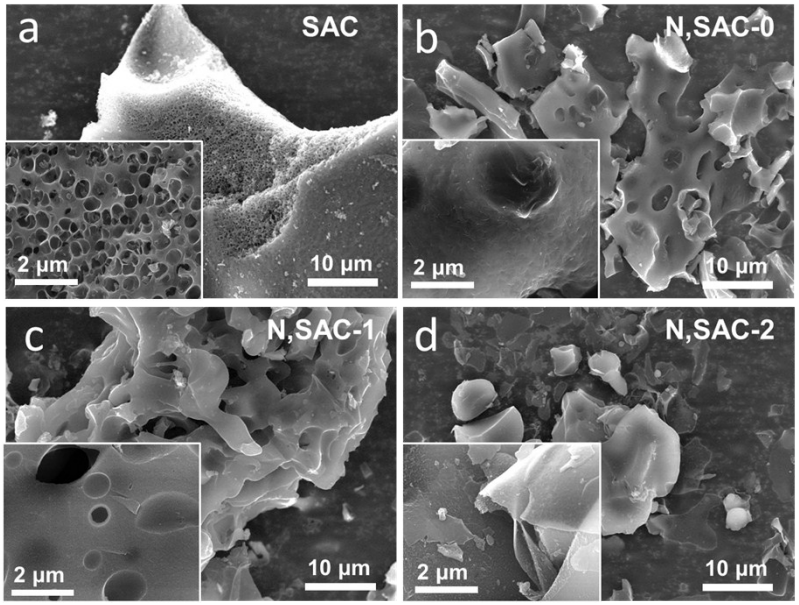

Figure S1. SEM micrographs of sodium alginate derived carbons: (a) SAC, (b) N,SAC-0, (c) N,SAC-1, and (d) N,SAC-2.

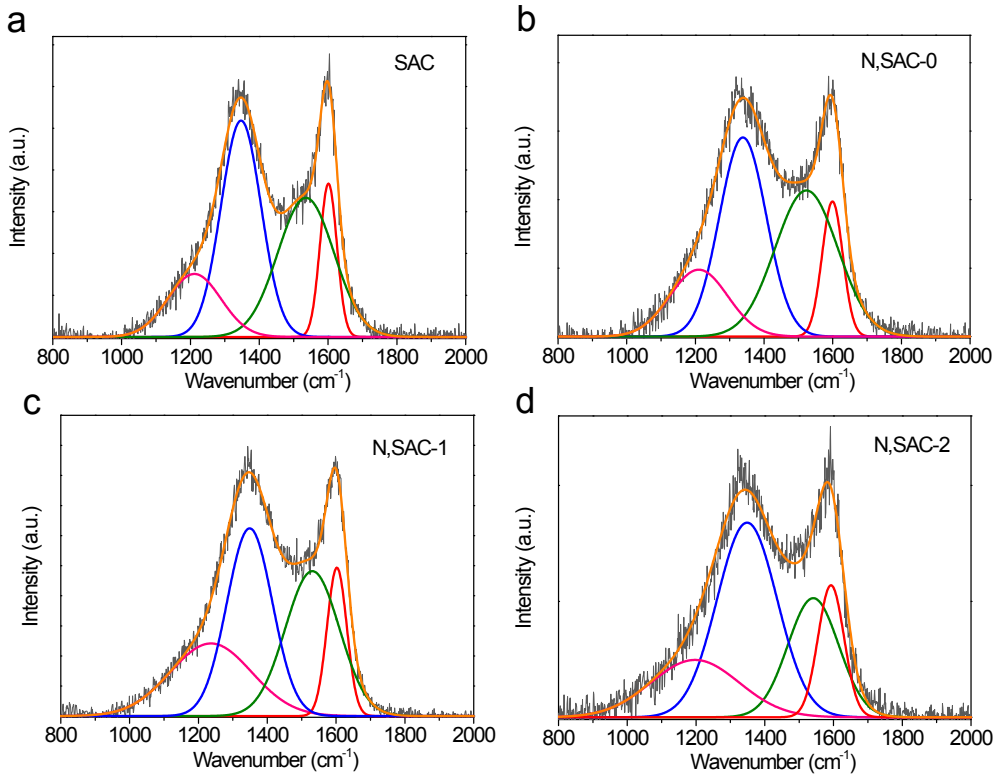

Figure S2. The fitted Raman spectra of all carbon specimens by using Voigt function.

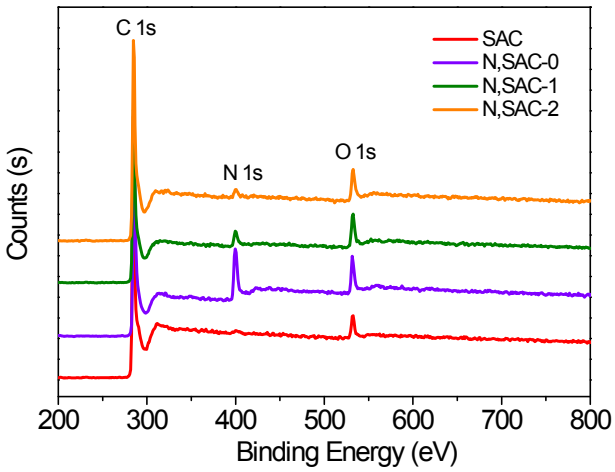

Figure S3. XPS survey spectra of all the samples.

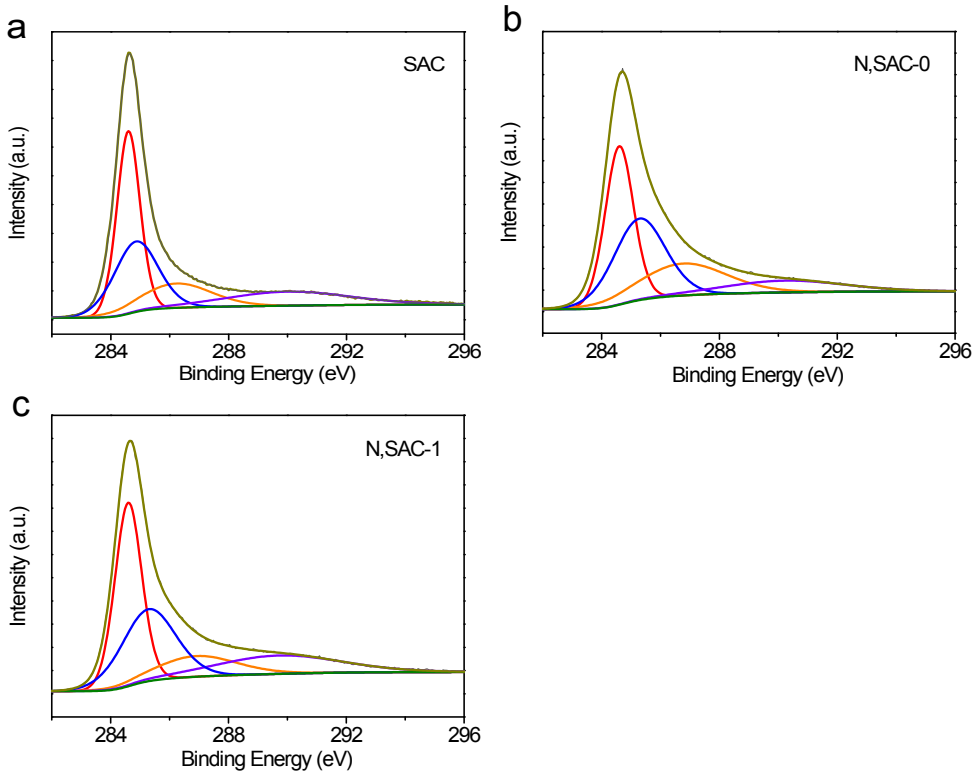

Figure S4. The high-resolution XPS C1s spectra of (a) SAC, (b) N,SAC-0, and (c) N,SAC-1.

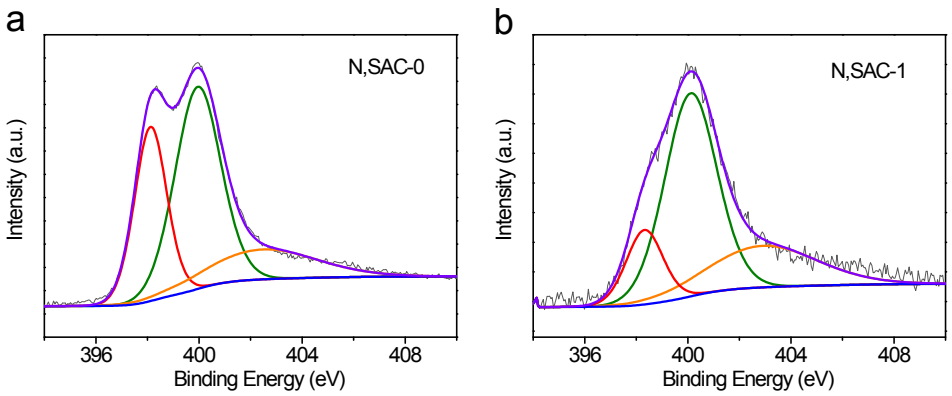

Figure S5. The high-resolution XPS N1s spectra of (a) N,SAC-0, and (b) N,SAC-1.

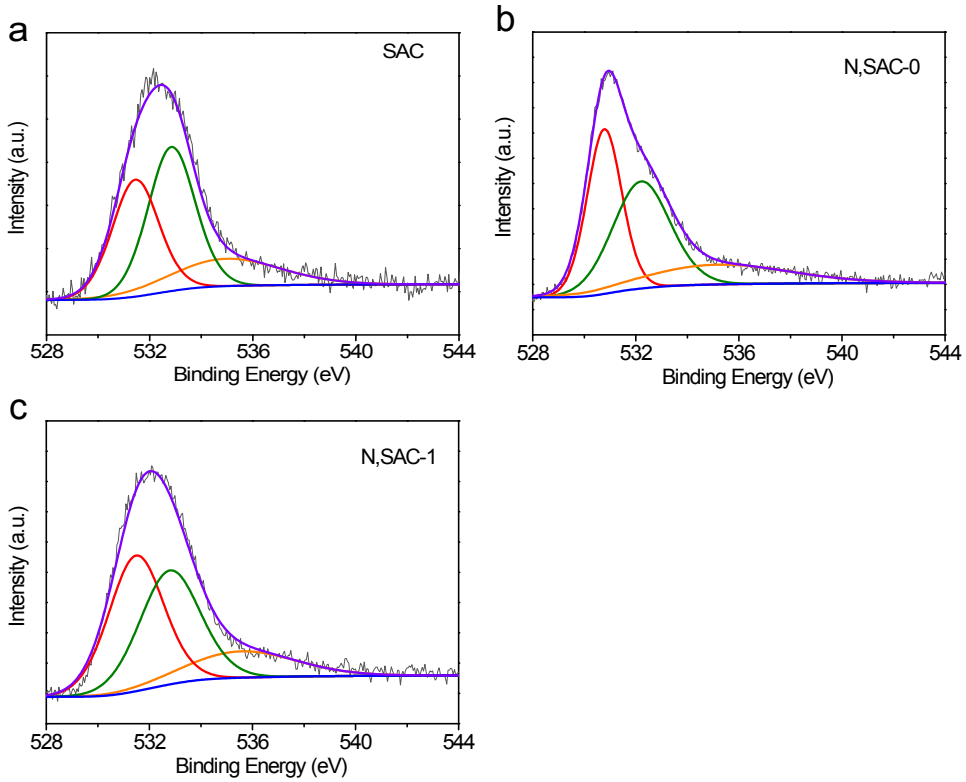

Figure S6. The high-resolution XPS O1s spectra of (a) SAC, (b) N,SAC-0, and (c) N,SAC-1.

Table S1 Relative surface concentrations (%) of nitrogen and oxygen species obtained by fitting N1s and O1s core level XPS spectra.

sample	N-6	N-5	N-Q	O-I	O-II	O-III
SAC	-	-	-	35.83	44.52	19.64
N,SAC-0	30.01	50.97	18.02	38.91	41.77	19.32
N,SAC-1	15.30	59.31	25.40	43.33	39.92	16.75
N,SAC-2	11.15	65.87	22.99	46.06	33.79	20.15

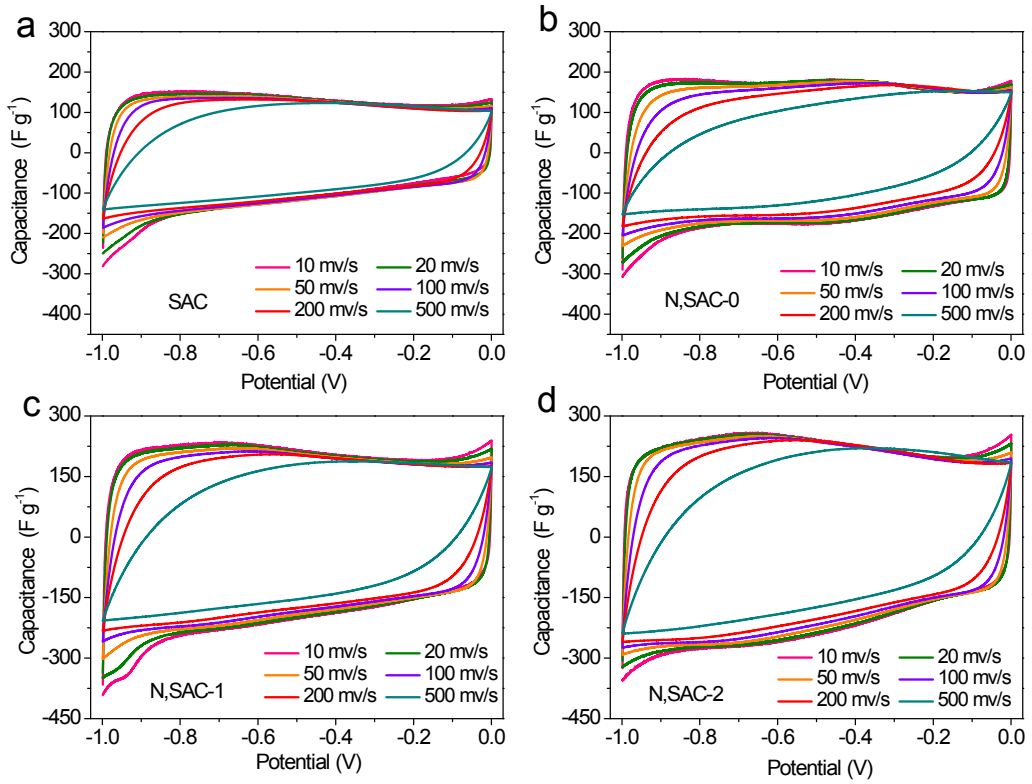

Figure S7. The CV curves of all the specimens for different scan rates in 2M KOH electrolyte.

Table S2 Comparison of capacitance and energy density of carbon-based electrodes for supercapacitors in KOH and/or ionic liquid electrolyte.

Sample	Heteroatom content	Capacity	Capacity retention	Cyclability	Energy at high power	Electrolyte
N,SAC-2 (this work)	N (7.2 wt%) O (7.4 wt%)	267 F g^{-1} (1 A g^{-1})	76.8% (1-100 A g^{-1})	97% after 10,000 cycles (10 A g^{-1})	-	2M KOH[a]
		188 F g^{-1} (1 A g^{-1})	56% (1-100 A g^{-1})	86.7% after 10,000 cycles (10 A g^{-1})	61 Wh kg^{-1} (373 W kg^{-1})	EMIM BF4[b]
Nitrogen-doped carbon nanosheets framework[1]	N (8.7 at%) O (7.2 at%)	242 F g^{-1} (1 A g^{-1})	83.4% (1-100 A g^{-1})	-	-	6M KOH[a]
		~143 F g^{-1} (1 A g^{-1})	50.7% (1-20 A g^{-1})	88.5% after 5,000 cycles (3 A g^{-1})	60.4 Wh kg^{-1} (1750 W kg^{-1})	EMIM BF4[b]
Platanus-derived hollow carbon micro-fibers[2]	N (1.23 at%) O (6.35 at%)	305 F g^{-1} (0.5 A g^{-1})	88.5% (0.5-10 A g^{-1})	97% after 10,000 cycles (4 A g^{-1})	-	6M KOH[a]
Porous nitrogen-doped hollow carbon spheres[3]	N (6.7 at%)	213 F g^{-1} (0.5 A g^{-1})	55.6% (0.5-10 A g^{-1})	91% after 5,000 cycles (1 A g^{-1})	-	6M KOH[a]
Willow-derived hollow carbon micro-fibers[2]	N (1.13 at%) O (7.63 at%)	276 F g^{-1} (0.5 A g^{-1})	81.1% (0.5-10 A g^{-1})	91% after 10,000 cycles (4 A g^{-1})	-	6M KOH[a]
Hierarchically porous carbon nanosheets[4]	N (1.6 at%) O (5.2 at%)	283 F g^{-1} (0.5 A g^{-1})	72% (0.5-50 A g^{-1})	95% after 20,000 cycles (20 A g^{-1})	-	6M KOH[a]
Pomegranate husk derived N-doped porous nanosheets carbon[5]	N (4.51 at%) H (0.76 at%)	254 F g^{-1} (0.5 A g^{-1})	73% (0.5-20 A g^{-1})	94.5% after 5,000 cycles	-	2M KOH[a]
Methyl cellulose based carbon nanosheets[6]	O (2.83-7.24 at%)	144 F g^{-1} (1 A g^{-1})	64% (1-100 A g^{-1})	91% after 20,000 cycles (10 A g^{-1})	18-44 Wh kg^{-1} (746 W k^{-1})	EMIM TFSI[b]
N, O-codoped hierarchical porous carbons[7]	N (0.64-0.85 at%) O (11.36-12.24 at%)	201 F g^{-1} (1 A g^{-1})	61% (1-100 A g^{-1})	91% after 10,000 cycles (10 A g^{-1})	62 W h kg^{-1} (750 W k^{-1})	EMIM BF4[b]
Hierarchical porous N-doped carbon[8]	N (3.8 wt%) O (6.7 wt%)	141 F g^{-1} (1 A g^{-1})	74% (1-80 A g^{-1})	93% after 10,000 cycles (10 A g^{-1})	59.8 Wh kg^{-1} (875 W kg^{-1})	EMI BF4[b]
N-doped		186 F g^{-1}		93% after 5,000		

mesoporous carbons[9]		(0.25 A g^{-1})		cycles (2 A g^{-1})		
3D nitrogen-doped porous carbon[10]	N (8.2 wt%) O (6.2 wt%)	156 F g^{-1} (0.5 A g^{-1})	58.5% (0.5-10 A g^{-1})	95.3% after 2,000 cycles (2 A g^{-1})	34.3 Wh kg^{-1} (313 W kg^{-1})	EMIM BF4/AN[b]

[a] Three-electrode system in 2M KOH electrolyte.

[b] Two-electrode symmetric supercapacitors in ionic liquid electrolyte.

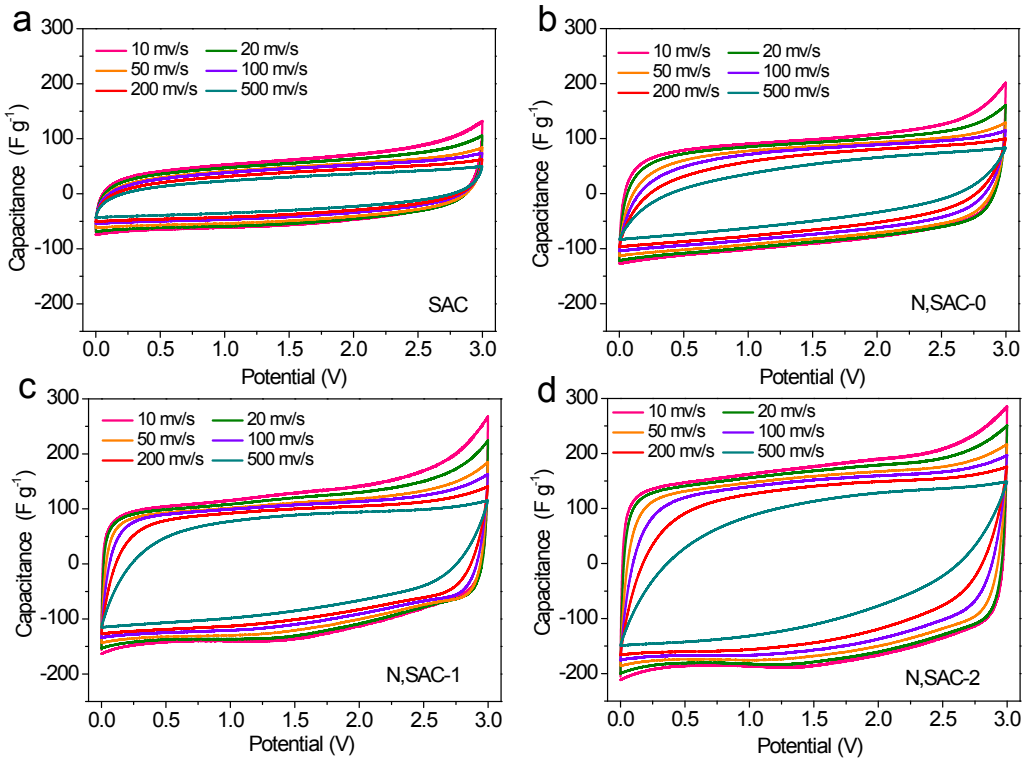

Figure S8. The CV curves of all the specimens for different scan rates in ionic liquid electrolyte.

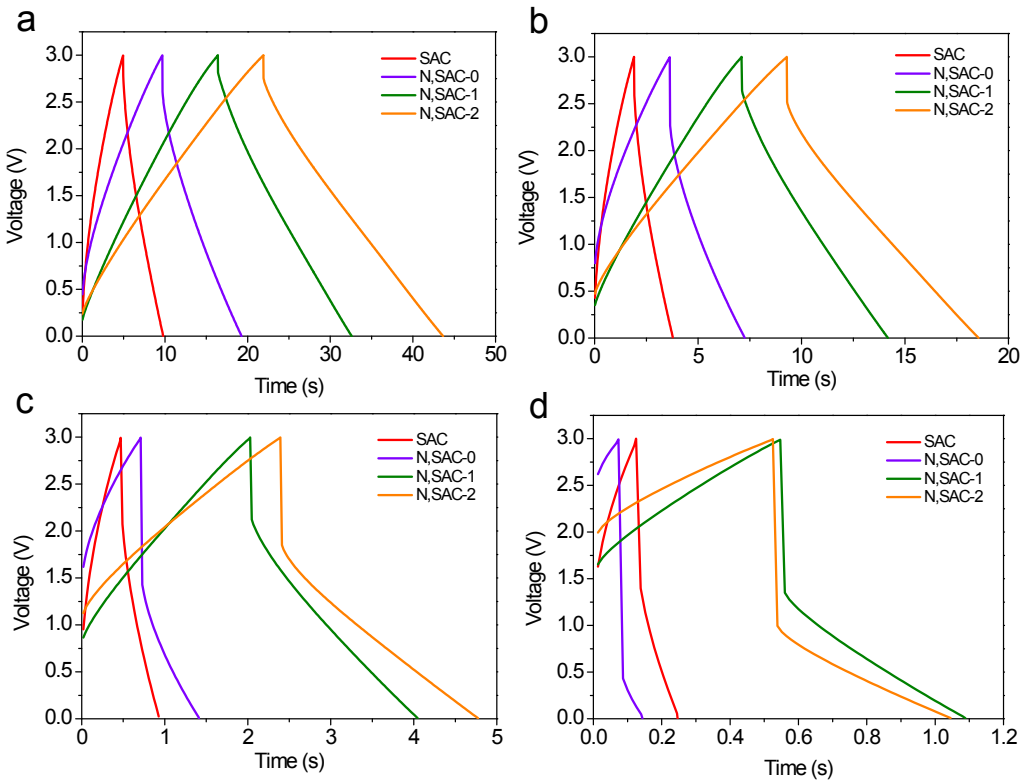

Figure S9. The galvanostatic charge-discharge curves of all samples measured at 10, 20, 50, and 100 A g^{-1} in ionic liquid electrolyte.

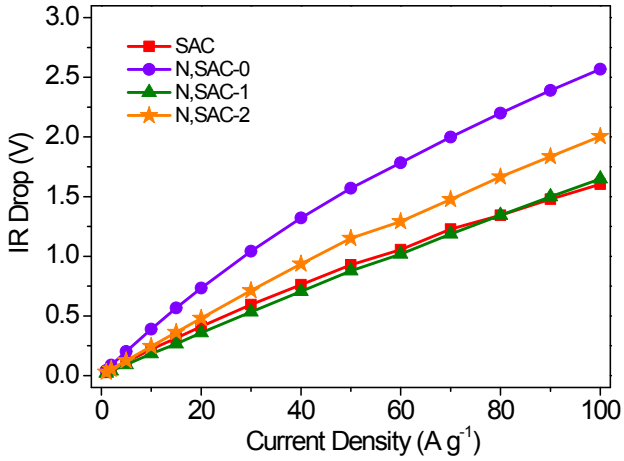

Figure S10. Potential IR drop vs. current density in ionic liquid electrolyte.

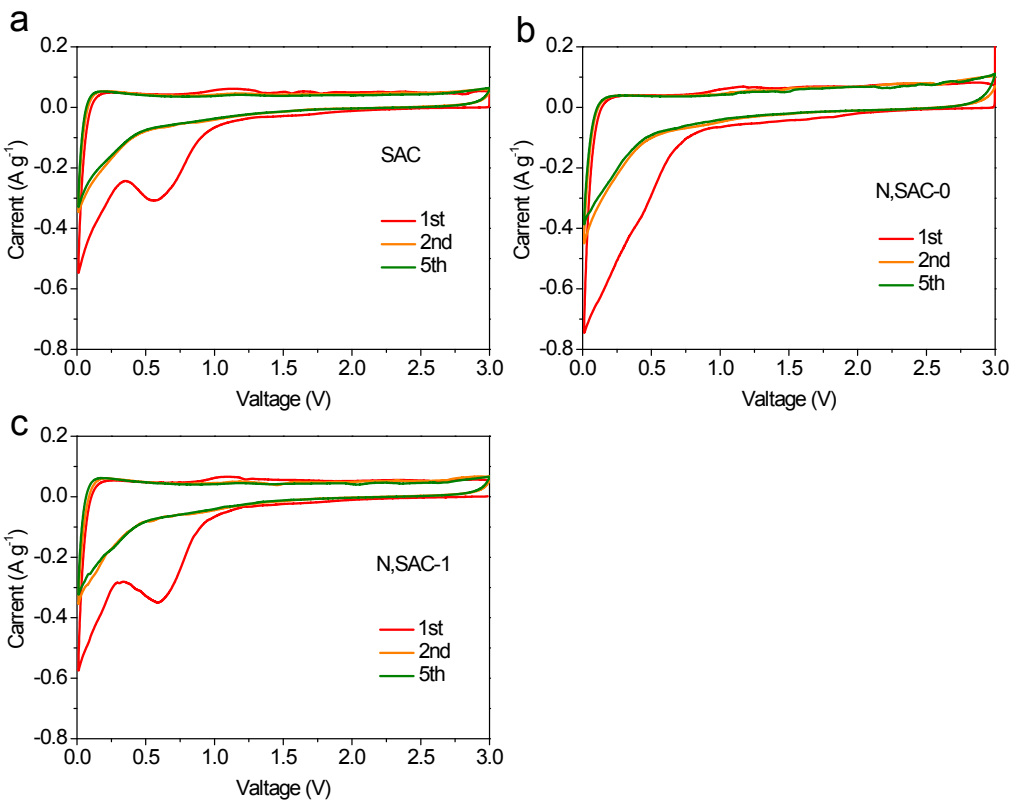

Figure S11. The CV curves of (a) SAC, (b) N,SAC-0, and (c) N,SAC-1 for lithium ion batteries.

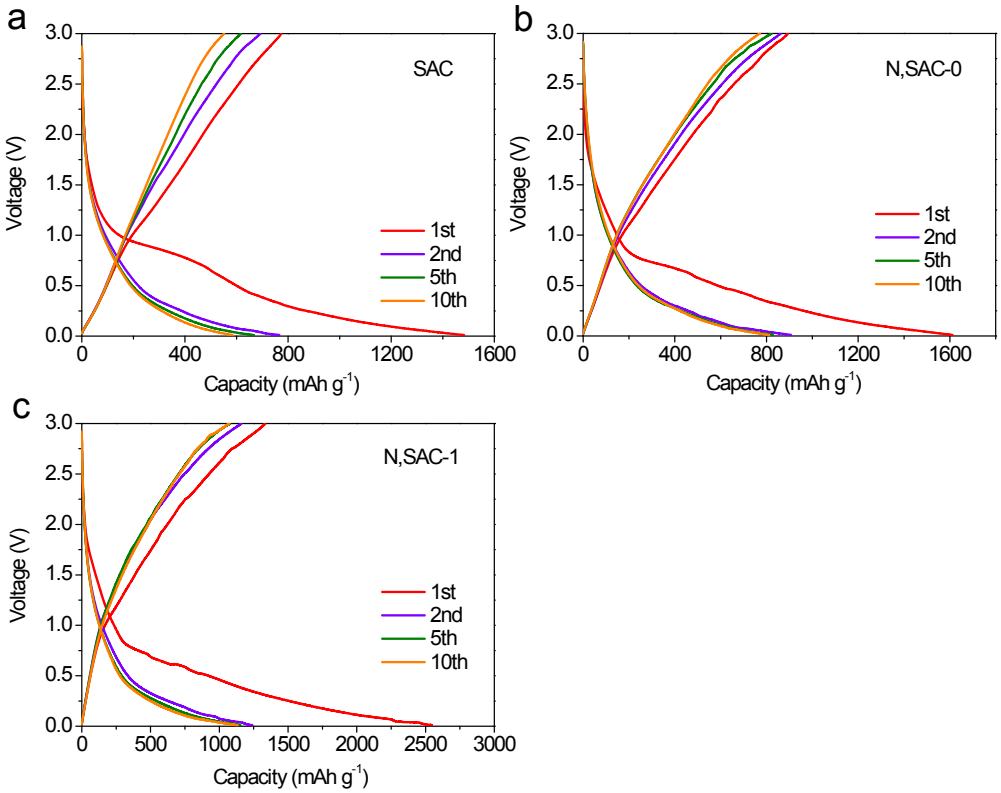

Figure S12. The galvanostatic charge-discharge curves of (a) SAC, (b) N,SAC-0, and (c) N,SAC-1 for lithium ion batteries.

Table S3 Comparison of capacity of carbon-based electrodes for lithium-ion battery anodes.

Sample	Heteroatom content	Initial coulombic efficiency	Rate capacity	Cyclability	Voltage	Electrolyte
N,SAC-2 (this work)	N (7.2 wt%) O (7.4 wt%)	51.4-55.4%	1455 mAh g^{-1} at 0.1 A g^{-1}; 604-658 mAh g^{-1} at 0.5 A g^{-1}; 223-233 mAh g^{-1} at 5 A g^{-1}; 162-173 mAh g^{-1} at 10 A g^{-1};	~300 mAh g^{-1} at 2 A g^{-1} after 500 cycles	0.01-3V	1 M $LiPF_6$
N, O-codoped hierarchical porous carbons[7]	N (0.64-0.85 at%) O (11.4-12.2 at%)	61-64%	900-1000 mAh g^{-1} at 0.1 A g^{-1}; 650 mAh g^{-1} at 0.5 A g^{-1}; 220 mAh g^{-1} at 5 A g^{-1}; 170 mAh g^{-1} at 10 A g^{-1};	350 mAh g^{-1} at 2 A g^{-1} after 500 cycles	0.01-3V	1 M $LiPF_6$
Nitrogen-doped carbon nanofiber aerogels[11]	N (7.3 at%) O (7.1 at%)	47%	630.7 mAh g^{-1} at 1 A g^{-1}; 485.8 mAh g^{-1} at 2 A g^{-1}; 392.9 mAh g^{-1} at 5 A g^{-1}; 327.5 mAh g^{-1} at 10 A g^{-1}; 289.0 mAh g^{-1} at 20 A g^{-1};	651 mAh g^{-1} at 1 A g^{-1} after 1000 cycles	0.01-3V	1 M $LiPF_6$
Nitrogen-Doped Hollow Carbon Nanospheres[12]	N (16.6 at%)	-	1945 mAh g^{-1} at 0.1 A g^{-1}; 1167 mAh g^{-1} at 3.2 A g^{-1}; 879 mAh g^{-1} at 5 A g^{-1};	879 mAh g^{-1} at 5 A g^{-1} after 1000 cycles	0.01-3V	1 M $LiPF_6$
Bio-derived hierarchically macro-meso-micro porous carbon[13]	N (5.3 wt%)	~62%	740 mAh g^{-1} at 0.1 A g^{-1}; 653 mAh g^{-1} at 0.2 A g^{-1}; 436 mAh g^{-1} at 0.8 A g^{-1}; 298 mAh g^{-1} at 1.6 A g^{-1}; 147 mAh g^{-1} at 2 A g^{-1};	470 mAh g^{-1} at 2C rate up to 150 cycles (1C rate is taken as 372 mAh g^{-1})	0.01-3V	$LiPF_6$ in 1:1 EC: DEC
Highly ordered mesoporous nitrogen-doped carbons[14]	N (3.57 at%) O (1.62 at%)	61%	1359 mAh g^{-1} at 0.1 A g^{-1}; 1137 mAh g^{-1} at 0.2 A g^{-1}; 847 mAh g^{-1} at 0.5 A g^{-1}; 726 mAh g^{-1} at 1 A g^{-1}; 592 mAh g^{-1} at 3 A g^{-1}; 435 mAh g^{-1} at 5 A g^{-1};	722 mAh g^{-1} at 1 A g^{-1} after 200 cycles	0.005-3V	1 M $LiPF_6$
Biomass waste inspired nitrogen-doped porous carbon materials[15]	N (4.31 at%) O (21.97 at%)	54.3%	1091 mAh g^{-1} at 0.1 A g^{-1}; 861 mAh g^{-1} at 0.2 A g^{-1}; 693 mAh g^{-1} at 0.4 A g^{-1}; 557 mAh g^{-1} at 0.8 A g^{-1}; 390 mAh g^{-1} at 1.6 A g^{-1};	1071 mAh g^{-1} at 0.1 A g^{-1} after 100 cycles 630 mAh g^{-1} at 1 A g^{-1} after 1000 cycles	0.01-3V	1 M $LiPF_6$

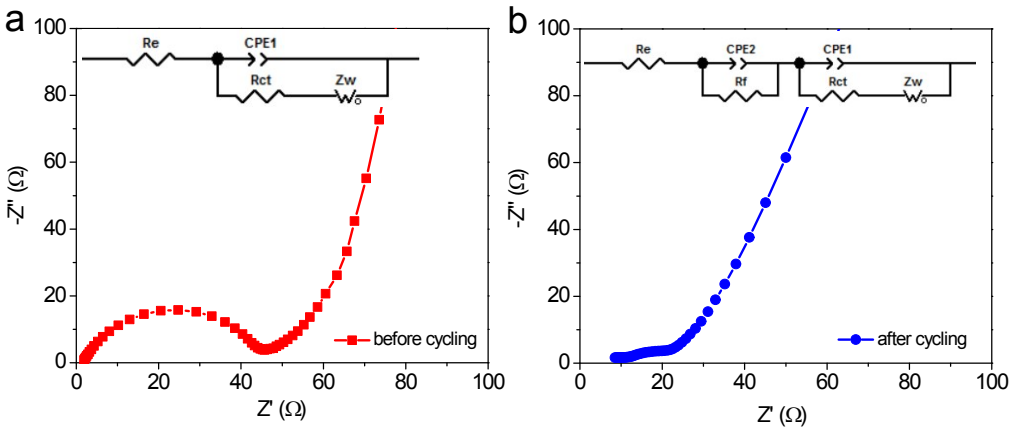

Figure S13. The Nyquist plots for N,SAC-2 (a) before cycling and (b) after 500 cycles.

References

1 Y. An, Y. Yang, Z. Hu, B. Guo, X. Wang, X. Yang, Q. Zhang and H. Wu, *J. Power Sources*, 2017, **337**, 45-53.

2 H. Tan, X. Wang, D. Jia, P. Hao, Y. Sang and H. Liu, *J. Mater. Chem. A*, 2017, **5**, 2580-2591.

3 J. Han, G. Xu, B. Ding, J. Pan, H. Dou and D. R. MacFarlane, *J. Mater. Chem. A*, 2014, **2**, 5352-5357.

4 Y. Cai, Y. Luo, H. Dong, X. Zhao, Y. Xiao, Y. Liang, H. Hu, Y. Liu and M. Zheng, *J.Power Sources*, 2017, **353**, 260-269.

5 K. Sun, J. Li, H. Peng, E. Feng, G. Ma and Z. Lei, *Ionics*, 2016, **23**, 985-996.

6 Y. Cui, H. Wang, N. Mao, W. Yu, J. Shi, M. Huang, W. Liu, S. Chen and X. Wang, *J. Power Sources*, 2017, **361**, 182-194.

7 W. H. Yu, H. L. Wang, S. Liu, N. Mao, X. Liu, J. Shi, W. Liu, S. G. Chen and X. Wang, *J. Mater. Chem. A*, 2016, **4**, 5973-5983.

8 L. Zhang, T. You, T. Zhou, X. Zhou and F. Xu, *ACS Appl. Mater. Interfaces*, 2016, **8**, 13918-13925.

9 D. Liu, C. Zeng, D. Qu, H. Tang, Y. Li, B.-L. Su and D. Qu, *J. Power Sources*, 2016, **321**, 143-154.

10 J. Pu, C. Li, L. Tang, T. Li, L. Ling, K. Zhang, Y. Xu, Q. Li and Y. Yao, *Carbon*, 2015, **94**, 650-660.

11 G. Ye, X. Zhu, S. Chen, D. Li, Y. Yin, Y. Lu, S. Komarneni and D. Yang, *J. Mater. Chem. A*, 2017, **5**, 8247-8254.

12 Y. Yang, S. Jin, Z. Zhang, Z. Du, H. Liu, J. Yang, H. Xu and H. Ji, *ACS Appl. Mater. Interfaces*, 2017, **9**, 14180-14186.

13 I. Elizabeth, B. P. Singh, S. Trikha and S. Gopukumar, *J. Power Sources*, 2016, **329**, 412-421.

14 Y. Zhang, L. Chen, Y. Meng, J. Xie, Y. Guo and D. Xiao, *J. Power Sources*, 2016, **335**, 20-30.

15 F. Zheng, D. Liu, G. Xia, Y. Yang, T. Liu, M. Wu and Q. Chen, *J. Alloys Compd*, 2017, **693**, 1197-1204.